Volume 1 | Number 1 | Jan 2013 | Pages 1–100

## Catalysis Science & Technology

www.rsc.org/catalysis

ROYAL SOCIETY OF CHEMISTRY

ROYAL SOCIETY OF CHEMISTRY

www.rsc.org/catalysis

**Mechanochemical preparation of advanced catalytically active bifunctional Pd-containing nanomaterials for aqueous phase hydrogenations**

Majd Al-Naji,[a] Alina M. Balu,[a,b]* Anca Roibu,[a] Michael Goepel,[a] Wolf-Dietrich Einicke,[a] Rafael Luque[c] and Roger Gläser[a]

[a]*Universitat Leipzig, Faculty of Chemistry and Mineralogy, Institute of Chemical Technology, Linnestaat 3, 04103 Leipzig, Germany.*

[b]*Department of Catalysis, New Chemistries Research Group, Avantium, Zekeringstraat 29, 1014 BV, Amsterdam, The Netherlands, e-mail: alina.balu@avantium.com*

[c]*Departamento de Química Orgánica, Facultad de Ciencias, Universidad de Córdoba Edificio Marie Curie (C3), Campus de Rabanales, Carretera Nacional IV-A, Km 396, E14014, email: q62alsor@uco.es*

*In memory of Prof. Juan M. Campelo, mentor of two Green Talents. This joint publication was possible as part of this award that is dedicated to him*

**Abstract**

The preparation of supported Pd nanoparticles on porous materials (Al-SBA-15 and Al-MCF) was successfully achieved using a simple, fast and efficient reactive milling (mechanochemical) method. Upon preparation, catalysts were characterized by $N_2$-physisorption, elemental analysis, Transmission Electron Microscopy (TEM) and X-ray diffraction (XRD). The catalytic activity of different Pd/Al-SBA-15 and Pd/Al-MCF materials was investigated in the hydrogenation of *p*-Nitrophenol (PNP) to *p*-Aminophenol (PAP) using $NaBH_4$ as reducing agent. Significant differences in catalytic activity for the prepared catalysts were observed, with a superior catalytic activity of Pd/Al-MCF as compared to Pd/Al-SBA-15. Furthermore, investigations on external mass-transfer limitations of the reaction conducted with two selected supported Pd catalysts were conducted and discussed.

## Introduction

Metallic nanoparticles have become a research topic of relevance in modern nanoscience due to their unique physico-chemical properties as well their important implications in catalytic processes.[1-5] As an example, the first work by Haruta *et al.*[6] on Au nanoparticles for CO oxidation was followed by a number of reports detailing the design of supported nanoparticle systems for heterogeneously catalyzed applications. In this regard, metal nanoparticles can be incorporated and supported in a number of porous supports using diverse techniques ranging from conventional methodologies such as incipient wetness impregnation or co-precipitation to more innovative protocols including ball milling,[7] microwave-assisted irradiation[8] or supercritical fluid reactive deposition (SFRD).[9, 10]

Functionalized nanoporous materials represent an important class of nanomaterials and a research area in which fascinating developments have been achieved in past decades.[11] One of current major challenges in the synthesis of nanoporous materials deals with the design and controllable preparation of a suitable porous structure with several complementary functions for improved activity, selectivity and stability in catalytic applications.[12-15] Ordered mesoporous SBA-15 silicas and mesostructured cellular foams (MCFs) are examples of porous solids able to provide most of the aforementioned requirements for an advanced catalytic material.

Mesostructured cellular foams (MCFs) comprise a novel type of porous silica-type materials comprising a three-dimensional structure with hydrothermally robust ultra-large mesopores (up to 50 nm).[16-18] In terms of textural and framework properties, MCFs are composed of uniform spherical cells interconnected by window pores with a narrow size distribution.[16] Owing to their 3D mesopore system with pore sizes substantially larger than those of SBA-15, these materials can be, in principle,

considered to be highly promising candidates as catalytic supports, potentially providing a faster diffusion of the reactants and products in chemical processes as well as a stable porous phase.[17,19] However, further functionalization is generally required to incorporate catalytically active sites into these materials due to their inherent inertness.[20-24]

The direct incorporation of metals into the structure of nanoporous silica supports can be achieved via isomorphic substitution of Si with Al, enabling the generation of acid sites. Interestingly, there is limited information about the functionalization of MCF materials for catalytic applications, with very few reports dealing with direct synthetic protocols, e.g., via isomorphic substitution.[25]

In this work, we present a simple, rapid and efficient alternative for metal incorporation into nanoporous supports based on reactive milling (mechanochemistry). Advanced bifunctional nano-molecular entities can be efficiently designed using this methodology, which provides accessibility to the active site of the catalysts in the reactions that require bifunctional catalysts i.e., acid sites as well as metal sites. This would be advantageous, e.g., for the conversion of biomass to liquid fuels and chemicals. The proposed methodology has been illustrated for the particular preparation and stabilization of Pd nanoparticles within two nanoporous aluminosilicate materials, i.e., Al-SBA-15 and Al-MCF. In addition to catalysts preparation, the catalytic activity of the prepared catalysts was assessed in greener aqueous-phase hydrogenations of aromatic compounds, using the low temperature (278 K) reduction of *p*-Nitrophenol (PNP) to *p*-Aminophenol (PAP) in presence of $NaBH_4$ as model test reaction.[26]

**Experimental Section**

*Catalyst preparation*

The synthesis of parent Al-SBA-15 support has been performed using a previously reported procedure[27] as follows: 25.2 g of structure directing agent (Pluronic P123, Sigma Aldrich) were dissolved in 472.5 mL of 2M HCl and 236 mL of distilled water. 54.9 g of (tetraethyl orthosilicate (TEOS), ABCR) and 2.8 g of aluminum isopropoxide (≥98% purity from Aldrich, corresponding to an Si/Al ratio 20 in the gel) were then added to the mixture and stirred at room temperature for 24 h at pH ≈ 2. This mixture was aged at 373 K for 24 h. The precipitated solid was filtered off, washed and dried at 373 K for 12 h prior to calcination at 873 K.

The synthesis of parent Al-MCF has comparably been adapted from Lettow *et al.* [17] 4.0 g Pluronic P123 (BASF, molecular weight = 5800) was dissolved in 22.8 g HCl (37%) and 75 mL distilled water. In contrast to the original procedure, 16 g 1,3,5 trimethylbenzene (MERK) (corresponding to a TMB/P123 ratio = 4) and 2.8 g aluminum isopropoxide were added to the solution. As silicon source, 8.8 g TEOS (ABCR) was added dropwise to the solution. Upon stirring at 310 K for 24 h and aging at 393 K in a closed Teflon bottle, the final obtained solid was filtered off, washed and calcined at 813 K to remove the remaining organics.

Supported Pd on Al-SBA-15 and Al-MCF catalysts were subsequently prepared using an efficient mechanochemical deposition of Pd onto the support material. In this method, certain amounts of the support (Al-SBA-15 and Al-MCF) and a metal precursor (palladium (II) acetate, Sigma Aldrich) in the solid phase were milled together for 5 min at 350 rpm using a planetary ball mill (Retsch PM 100 model). For comparison, a supported Pd on Al-MCF catalyst was prepared via conventional

incipient wetness impregnation (IWI) with 0.5 wt.% of Pd as an aimed loading. The

required amount of tetraamminepalladium (II) nitrate (Sigma Aldrich) was dissolved in

distilled water and added dropwise with continuous stirring to the support, i.e., Al-MCF.

The obtained catalysts were calcined for 4 h at 723 K and reduced under a flow of $H_2$ (2

mL min$^{-1}$) in $N_2$ (8 mL min$^{-1}$). The incorporation procedure is illustrated in Figure 1.
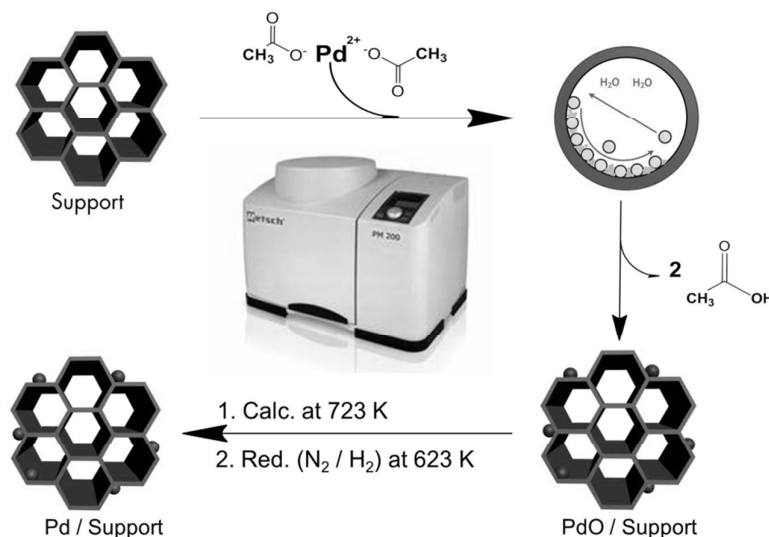


Figure 1. Scheme representing the incorporation of Pd nanoparticles onto ordered

nanoporous material (Al-SBA-15 and Al-MCF) via ball milling.

*Characterization techniques*

The prepared catalysts were characterized by $N_2$-physisorption, elemental

analysis, transmission electron microscopy (TEM) and X-ray diffraction (XRD). The

specific surface area, pore volume and pore size distribution were determined using a

micrometrics ASAP 2010 apparatus. The metal content was determined by optical

emission spectroscopy with inductively coupled plasma (ICP-OES) after dissolution of

the sample in aqueous $HNO_3$/HF solution using a Vario EL-Heraeus microanalyzer.

Transmission Electron Micrographs (TEM) of the support materials and the catalysts

were recorded on a JEOL JEM 2010HR instrument operated at 300 kV. Samples were suspended in ethanol and deposited straightaway on a copper grid prior to analysis. EDX for elemental analysis could also be recorded on the same apparatus. Additionally, XRD patterns were recorded within $2\theta = 4 - 90°$ range using a Siemens, D5000 diffractometer (0.05° counts per step) and Cu-K$\alpha$ radiation ($\lambda = 0.154$ nm).

*Catalytic test reaction*

The catalytic hydrogenation of PNP to PAP was carried out in a 100 mL batch reactor at 279 K (ambient pressure, 1300 rpm stirring speed). Figure 2 depicts the catalytic experimental setup. Details of the experimental procedure may be found elsewhere.[26] In brief, 5 mL of an aqueous solution of $NaBH_4$ (0.60 mmol$^{-1}$) were added to 45 mL of an aqueous solution of PNP (0.18 mmol$^{-1}$). The reaction was started by introducing 0.07 g of the reduced catalyst. PNP concentration changes were monitored via on-line UV-vis spectroscopy (AvaSpec-3648, optical path length: 5 mm) at a wavelength of 400 nm. The initial reaction rate ($r_0$) was calculated by assuming first order reaction from the linear decrease of PNP concentration after the addition of the catalyst.



Figure 2. Experimental setup for hydrogenation of PNP with $NaBH_4$ to PAP with online UV-vis spectrometer.

**Results and Discussion**

*Material preparation and characterization*

Pd nanoparticles have been incorporated into the support via ball milling, following a previously established methodology[7], in two steps, namely hydrolysis of the metal precursor to generate $Pd^{2+}$ species (PdO, upon calcination) followed by subsequent reduction to $Pd^0$ nanoparticles. The protocol allows the incorporation of an uniform distribution of Pd nanoparticles mostly on the surface of the support, with a contribution within the pores of the materials as previously reported.[27, 28]

Textural properties of the synthesized materials are summarized in Table 1 and Figure 3. In all cases, isotherms were found to be of type IV with hysteresis loops of H1 type according to the IUPAC classification. These correspond to mesoporous materials with pores of the same cross section (for instance, cylindrical or hexagonal). Pore-filling steps in adsorption and desorption curves were sharp, corresponding to a narrow pore size distribution. Specific surface area ($S_{BET}$), specific surface area for micropores ($S_{mi}$), specific pore volume for micropores and mesopores ($V_{mi}$ and $V_{me}$), total pore volume ($V_{tot}$) at relative pressure 0.99, and pore diameter ($d_p$) and window diameter ($d_w$) obtained from desorption branch of the isotherms are summarized in Table 1.

No major changes could be observed in terms of textural properties upon Pd incorporation into Al-SBA-15 or Al-MCF. Specific surface areas generally decreased with the amount of incorporated Pd (up to a maximum of 20 %) as expected, with an interesting decrease in the micropore contribution for Al-SBA-15 materials (Table 1, $S_{mi}$ column). The decrease in micropore surface area may be due to micropore filling with Pd, although a contribution of micropore destruction from the milling process cannot be ruled out. Comparably, an unexpected increase in micropore surface area

could be observed for ball-milled Al-MCF materials which can be attributed to micropore opening after milling of unnacessible micropores already present in the original Al-MCF (unquantified via adsorption in the parent material). Pore diameters were only slightly reduced upon Pd incorporation, i.e. minimum generation of Pd nanoparticles within the pores of the materials, without any significant changes in $V_{tot}$. These findings again confirmed the predominant deposition of Pd NPs on the external surface of the support in good agreement with previous results of Luque *et al*.[7, 11, 28]

**Table 1.** Textural properties of materials synthesized in this work include specific surface area ($S_{BET}$), specific surface area for micropores ($S_{mi}$), pore volume for micropores and mesopores ($V_{mi}$ and $V_{me}$), total pore volume ($V_{tot.}$), window diameter ($d_w$) and Pd content and Al content (measured by ICP-OES).

| Materials | $S_{BET}$ $(m^2g^{-1})$ | $S_{mi}$ $(m^2g^{-1})$ | $V_{mi}$ $(cm^3g^{-1})$ | $V_{me}$ $(cm^3g^{-1})$ | $V_{tot.}$ $(cm^3g^{-1})$ | $d_p$ (nm) | $d_w$ (nm) | Al content (wt.%) |
|---|---|---|---|---|---|---|---|---|
| Al-SBA-15 | 728 | 230 | 0.09 | 0.5 | 0.6 | 9.8 | - | 2.0 |
| 0.2 Pd/Al-SBA-15 | 715 | 113 | 0.04 | 0.5 | 0.6 | 7.3 | - | 1.7 |
| 2.0 Pd/Al-SBA-15 | 736 | 105 | 0.04 | 0.6 | 0.7 | 6.8 | - | 2.2 |
| Al-MCF | 693 | 148 | 0.06 | 2.1 | 2.1 | 28.0 | 15.0 | 0.2 |
| 0.4 Pd/Al-MCF | 616 | 152 | 0.06 | 2.0 | 2.1 | 26.0 | 14.0 | 0.8 |
| 2.1 Pd/Al-MCF | 579 | 175 | 0.07 | 2.0 | 2.1 | 25.0 | 14.0 | 0.2 |

The amount of Pd loading on the support was determined by elemental analysis via ICP-OES. Catalysts studied in this work were originally prepared with 0.5 wt.% and 2.0 wt.% aimed Pd loadings, which correlated fairly well with actual Pd loadings in the final materials. Only for the case of 0.5 Pd/Al-SBA-15, the final Pd loading was found to be rather low (0.2 wt.%). Pd and Al content in all materials are included in Table 1.
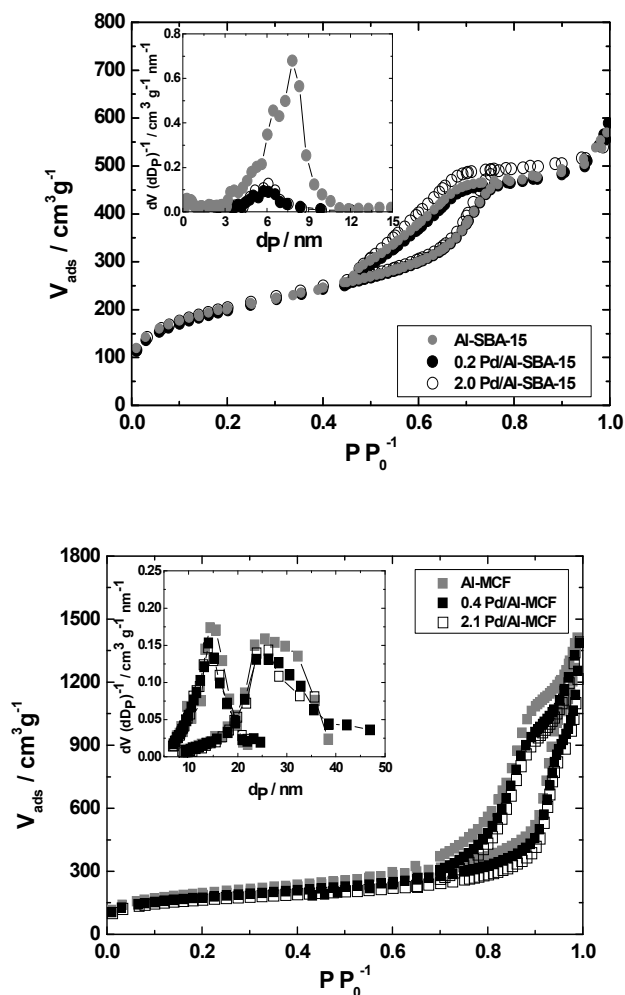
**Figure 3**. Nitrogen physisorption isotherms at 77 K and pore width distribution determined using the BJH method on the desorption branch of the isotherm for Al-SBA-15, 0.2 Pd/Al-SBA-15 and 2.1 Pd/Al-SBA-15 (top plot); Al-MCF, 0.4 Pd/Al-MCF and 2.1 Pd/Al-MCF (bottom plot).

TEM images for 0.2 Pd/Al-SBA-15 and 0.4 Pd/Al-MCF have been shown in Figure 4. Pd-containing Al-SBA-15 materials exhibited the characteristic highly ordered hexagonal arrays of mesopores with large uniform pore diameters and a well preserved structure after ball milling and Pd incorporation. In contrast, TEM images revealed a

disordered array of silica sturts containing uniform spherical cells interconnected by windows with a narrow size distribution, all characteristic of MCF materials.[29] Images did not allow a clear visualization of Pd nanoparticles (Figure 4) which in any case rules out the presence of large Pd clusters in the materials. XRD patterns (Figure S1 in ESI) of the prepared catalysts did not reveal any characteristic Pd diffraction lines (even for samples with 2.0 wt.% Pd loading), as expected due to the low Pd content in the materials and their high dispersion on the supports. These results were in good agreement with TEM results which did not show any clear Pd nanoparticles in the materials.
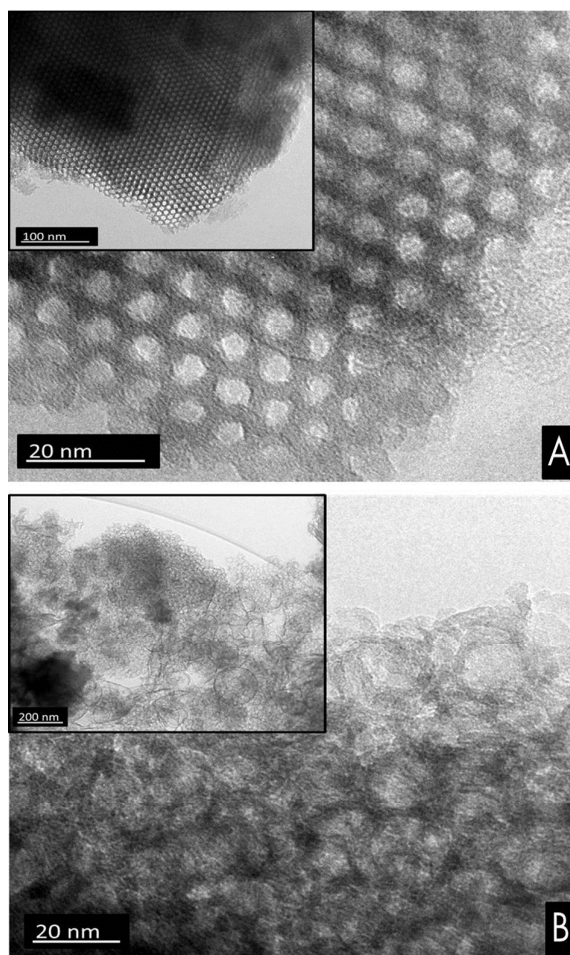


**Figure 4.** Representative TEM images of prepared catalysts (A) 0.2 Pd/Al-SBA-15 (B) 0.4 Pd/Al-MCF.

*Catalytic activity*

Catalytic experiments of Pd-containing Al-SBA-15 and Al-MCF materials in the aqueous hydrogenation of PNP to PAP at 278 K using $NaBH_4$ as reducing agent were conducted. Results are depicted in Figures 5 to 8. PNP adsorption on Al-SBA-15 and Al-MCF supports materials as well the effects of the support on PNP hydrogenation were initially investigated. The addition of the support material did not have any significant influence on the observed PNP concentration, ruling out any significant adsorption effects on the catalytic measurements. Moreover, experiments in the presence of parent Al-SBA-15 and Al-MCF supports and in the absence of any solid material (blank runs) gave no catalytic activity, i.e., no PNP concentration change in solution was observed. Upon addition of the Pd-containing catalysts, PNP concentration decreased linearly with time, reaching a maximum conversion after less than 5 min. Figure 5 summarizes the results of concentration vs. time behavior for the investigated catalysts. Almost quantitative conversion could be achieved for 2.0 Pd/Al-SBA-15 and 2.1 Pd/Al-MCF in a very short period of time (typically less than 2 minutes).
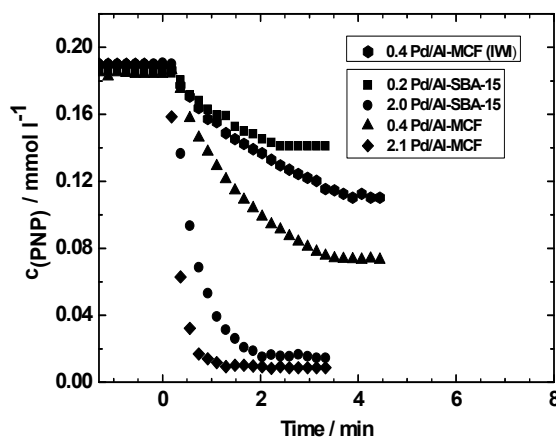


**Figure 5.** Concentration of PNP as a function of time for different supported Pd catalysts in the hydrogenation of PNP to PAP using $NaBH_4$ as reducing agent. ($c_{(PNP)}$ =

$0.18$ mmol L$^{-1}$, $c_{(NaBH4)} = 0.60$ mmol L$^{-1}$, T $= 279$ K, stirring speed $= 1300$ min$^{-1}$, $m_{catalyst}$ $= 0.07$ g).

As expected, rates of reactions were slower for lower Pd loaded materials, although a highly promising ca. 60% conversion was achieved for 0.4 Pd/Al-MCF after 5 minutes of reaction (Figure 5).

Note that on catalysts with lower loading and from IWI, a complete conversion of PNP to PAP was not achieved. This is, however, not due to catalyst deactivation, but due to incomplete utilization of the hydrogen from NaBH4 decomposition in the PNP hydrogenation. In fact, complete conversion can be reached also on these less active catalysts, if more NaBH4 is added to the reaction mixture (see Figure S3 in ESI).[26]

Initial reaction rates were subsequently calculated by assuming a first order reaction, from the linear decrease of PNP concentration as function of time after addition of the catalyst (Figure 6). The generally higher reaction rate for 2.0 Pd/Al-SBA-15 (0.220 mmol l$^{-1}$ min$^{-1}$) as compared to 0.2 Pd/Al-SBA-15 (0.019 mmol l$^{-1}$ min$^{-1}$) and 2.1 Pd/Al-MCF (0.306 mmol l$^{-1}$ min$^{-1}$) as compared to 0.4 Pd/Al-MCF (0.137 mmol l$^{-1}$ min$^{-1}$) can be easily correlated to their respectively larger Pd content. A linear correlation of such higher rates of reaction with the quantity of Pd in the materials was not observed which may be due to more severe mass-transfer limitations for increasing initial reaction rates (see below). The initial reaction rates determined in this work were comparably superior to those previously reported by Goepel *et al.* using similarly loaded supported Pt catalysts.[26] Results were also consistent and in good agreement with findings from El-Sheikh *et al.*[29], who also reported a higher catalytic performance of supported Pd as compared to supported Pt catalysts in NaBH$_4$-mediated PNP

hydrogenation. However, Goepel *et al.*[26] observed a limitation of reaction kinetics by internal mass-transfer effects. The increase in initial reaction rate compared to the supported Pt-catalysts used in their study (prepared by electrostatic adsorption) can also be understood as overcoming internal mass-transfer limitations via preferential deposition of Pd on the external surface of the catalyst,[28] illustrating the advantages of mechanochemical catalyst preparation.
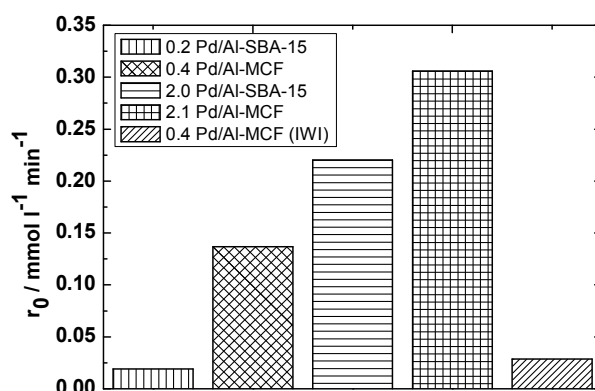


**Figure 6.** Initial reaction rates in the hydrogenation of PNP to PAP using $NaBH_4$ as reducing agent for different supported Pd catalysts. ($c_{(PNP)}$ = 0.18 mmol $l^{-1}$, $c_{(NaBH4)}$ = 0.60 mmol $l^{-1}$, T = 279 K, stirring speed = 1300 $min^{-1}$, $m_{catalyst}$ = 0.07 g).

In order to compare catalytic results achieved with ball milling-prepared supported Pd nanoparticles with conventionally prepared catalysts, a similarly low loaded 0.4 Pd/Al-MCF catalyst prepared via IWI was used. As expected, the conversion was much faster when using 0.4 Pd/Al-MCF (Figure 5, dotted line) prepared by ball milling compared to the catalyst with the same Pd loading obtained by IWI. Only the conversion over the catalyst 0.2 Pd/Al-SBA-15 prepared via ball milling is slower. This can be attributed to its lower noble metal loading. These findings are in good agreement

with previous results from the group[27, 28] and confirm the remarkable possibilities of mechanochemically synthesized materials as advanced catalysts.

Mass-transfer limitations in the aqueous phase were finally evaluated in the systems. With this purpose, the stirring speed was varied for the conversion using two selected catalysts, i.e., 0.2 Pd/Al-SBA-15 and 0.4 Pd/Al-MCF. A linear correlation between stirring speed and initial rate of reaction was observed for both catalysts (Figure 7), confirming that the hydrogenation of PNP using $NaBH_4$ as a reducing agent is limited by external mass-transfer. Similarly, external mass-transfer limitations were also found for very active Pt catalysts supported on mesoporous silica gel.[26] These results may indicate that the Pd particles are highly dispersed (< 2 nm) on the external surface of the support. The fact that the initial reaction rate is higher for the higher metal loadings is also consistent with the above mentioned conclusion that most of Pd particles are located at the external surface in the supports. For both lower and higher Pd loading, Al-MCF-based catalysts were more active as compared to Al-SBA-15.

In view of the observed external mass-transfer limitations, Al-MCF-base catalysts can be proposed to either contain smaller Pd particles, i.e., supports a higher Pd dispersion, or it comprises smaller or differently shaped grains resulting in a thinner diffusion layer and consequently a less pronounced external mass-transfer limitation of the reaction rates.

The stability of synthesized Pd catalysts was also investigated in this work. ICP/OES of both filtrate (no Pd leaching detected in solution, <0.5 ppm) as well as the reused catalyst (0.4 wt.% Pd in the reused catalyst, identical to 0.4 wt.% Pd measured in fresh Pd/Al-MCF) supports the high stability of recyclability of mechanochemically synthesized nanocatalysts in aqueous room temperature catalytic processes, in good agreement with recent reports.[29]
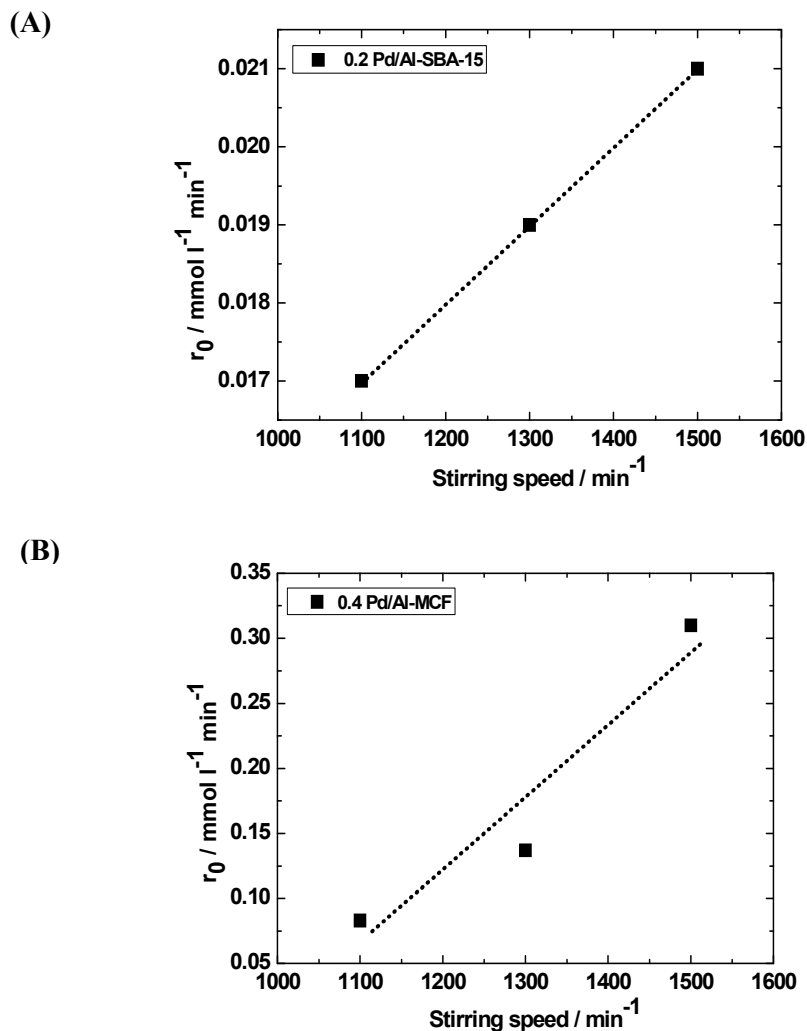
**(A)**



**(B)**



**Figure 7.** Initial reaction rate ($r_0$) dependence with stirring speed in the hydrogenation of PNP to PAP using $NaBH_4$ as a reducing agent (A) 0.2 Pd/Al-SBA-15 and (B) for 0.4 Pd/Al-MCF. ($c_{(PNP)}$ = 0.18 mmol $l^{-1}$, $c_{(NaBH4)}$ = 0.60 mmol $l^{-1}$, T = 279 K, stirring speed = 1300 $min^{-1}$, $m_{catalyst}$ = 0.07 g).

**Conclusions**

Advanced bifunctional nanomaterials Pd/Al-SBA-15 and Pd/Al-MCF have been successfully designed using a facile and straightforward route based on a dry milling mechanochemical protocol as innovative preparation strategy. The catalytic activity as

well as the mass-transfer limitations of the prepared catalysts have been successfully investigated in the hydrogenation PNP to PAP as a model reaction. Significant differences in catalytic activity for the prepared catalysts were observed, with an optimum activity achieved for 2.1 Pd/Al-MCF and negligible activities obtained for similar materials prepared via conventional incipient wetness impregnation (IWI) method. The new generation of advanced mechanochemically synthesized materials is envisaged to pave the way to the utilization of simple, stable and highly active nanomaterials for challenging catalytic processes (e.g. aqueous chemistries) within future biorefineries and biomass processing.

**Acknowledgements**

**References**

[1]    P. Hervés, M. P. Lorenzo, L. M. L. Marzán, J. Dzubiella, Y. Lu, M. Ballauff, *Chem. Soc. Rev.* **2012,** *41*, 5577- 5587.

[2]    A. A. Ismaila, A. Hakki, D. W. Bahnemann, *J. Mol. Catal. A: Chem.* **2012**, *358*, 145-151.

[3]    Y. Mei, Y. Lu, F. Polzer, M. Ballauff, *Chem. Mater.* **2007,**  *19*, 1062-1069.

[4]    Y. Lu, Y. Mei, M. Drechsler, M. Ballauff, *Angew. Chem. Int. Ed.* **2006**, *45* 813- 816.

[5]    W. Schäartl, *Nanoscale* **2010**, *2*, 829-843.

[6]    M. Haruta, T. Kobayashi, H. Sano, N. Yamada, *Chem. Lett.* **1987**, *2*, 405-408.

[7]    A. Pineda, A. M. Balu, J. M. Campelo, A. A. Romero, D. Carmona, F.   Balas, J. Santamaria, R. Luque*, ChemSusChem* **2011***, 4,* 1561-1565*.*

[8]    A. M. Balu, D. Dallinger, D. Obermayer, J. M. Campelo, A. A. Romero, D. Carmona, F. Balas, K. Yoshida, P. L. Gai, C. Vargas, C. O. Kappe, R. Luque, *Green Chemistry* **2012**, *14*, 393-402.

[9]    J. Morère, M. J. Tenorio, M. J. Torralvo, C. Pando, J. A. R. Renuncio, A. Cabañas, *J. Supercrit. fluids* **2011**, 65, 213-222.

[10]   M. Lindo, A. J. Vizcaíno, J. A. Calles, A. Carrero, *Int. J. Hydrogen Energy* **2010**, *35*, 5895-5901.

[11]   M. Ojeda, A.M. Balu, V. Barrón, A. Pineda, A. Garcia, A. A. Romero, R. Luque, *J. Mater. Chem. A* **2014,** *2*, 387-393.

[12]   V. Salgueiriño-Maceira, M. A. Correa-Duarte, *Adv. Mater.* **2007,** *19*, 4131-4144.

[13]   P. Majewski, B. Thierry, *Crit. Rev. Solid State Mater. Sci.* **2007**, *32,* 203-215.

[14]    P. Tallury, K. Payton, S. Santra, *Nanomedicine* **2008**, *3*, 579-592.

[15]   J. Kim, Y. Piao, T. Hyeon, *Chem. Soc. Rev.* **2009**, *38*, 372-390.

[16]  P. S. Winkel, W. W. Lukens, D. Zhao, P. Yang, B. F. Chmelka, G. D. Stucky, *J. Am. Chem. Soc.* **1999**, *121*, 254-255

[17]  J. S. Lettow, Y. J. Han, P. S. Winkel, P. Yang, D. Zhao, G. D. Stucky, J. Y. Ying, *Langmuir* **2000**, *16*, 8291-8295

[18]  Q. Li, Z. Wu, D. F. Eng, B. Tu, D. J. Zhao, *J. Phys. Chem. C* **2010**, *11*, 5012-5019.

[19]  Y. J. Han, J. T. Watson, G. D. Stucky and A. Butler, *J. Mol. Catal. B* **2002**, *1*, 1-8.

[20]  C. Li, Y. Wang, Y. Guo, X. Liu, Y. Guo, Z. Zhang, Y. Wang, G. Lu, *Chem. Mater.* **2007**, *19,* 173-178.

[21]  Z. Lihui, H. Jun, X. Songhai, L Honglai, *Chin. J. Chem. Eng.* **2007**, *15*, 507-511.

[22]  A. Galarneau, H. Cambon, F. Di Renzo, F. Fajula, *Langmuir* **2001**, *17,* 8328-8335.

[23]  Y. M. Liu, J. Xu, L. C. Wang, Y. Cao, H. Y. He, K. N. Fan, *Catal Lett.* **2008**, 125, 62-68.

[24]  R. Fazaeli, H. Aliyan, M. A. Ahmadi, S. Hashemian, *Catal. Commun.* **2012**, *29,* 48-52.

[25]  L. Hermida, A. Abdullah, A. Mohamed, *Mater. Sci. Appl.* **2013**, 4, 52-62.

[26]  M. Goepel, M. Al-Naji, P. With, G. Wagner, O. Oeckler, D. Enke, R. Gläser, *Chem. Eng. Technol.* **2014**, *37*, 551-554.

[27]  a) A. M. Balu, A. Pineda, K. Yoshida, J. M. Campelo, P. L. Gai, R. Luque, A. A. Romero, *Chem. Commun.* **2010**, *46*, 7825-7827; b) A. M. Balu, A. Pineda, D. Obermayer, A. A. Romero, C. O. Kappe, R. Luque, *RSC Adv.* **2013**, *3*, 16292-16295.

[28]  a) M. Ojeda, A. M. Balu, V. Barron, A. Pineda, A. Garcia, A. A. Romero, R. Luque, *J. Mater Chem. A* **2014**, *2*, 387-393; b) M. Ojeda, A. Pineda, A. A. Romero, V. Barron, R. Luque, *ChemSusChem* **2014**, 10.1002/cssc.201400055.

[29]  S. M. El-Sheikh, A. A. Ismail, J. F. Al-Sharab, *New J. Chem.* **2013**, *37*, 2399-2407.

**Mechanochemical preparation of advanced catalytically active bifunctional Pd-containing nanomaterials for aqueous phase hydrogenations**

Majd Al-Naji,[a] Alina M. Balu,[a,b]* Anca Roibu,[a] Michael Goepel,[a] Wolf-Dietrich Einicke,[a] Rafael Luque[c] and Roger Gläser[a]

[a]*Universitat Leipzig, Faculty of Chemistry and Mineralogy, Institute of Chemical Technology, Linnestaat 3, 04103 Leipzig, Germany.*

[b]*Department of Catalysis, New Chemistries Research Group, Avantium, Zekeringstraat 29, 1014 BV, Amsterdam, The Netherlands, e-mail: alina.balu@avantium.com*

[c]*Departamento de Química Orgánica, Facultad de Ciencias, Universidad de Córdoba Edificio Marie Curie (C3), Campus de Rabanales, Carretera Nacional IV-A, Km 396, E14014, email: q62alsor@uco.es*

*In memory of Prof. Juan M. Campelo, mentor of two Green Talents. This joint publication was possible as part of this award that is dedicated to him*

**Abstract**

The preparation of supported Pd nanoparticles on porous materials (Al-SBA-15 and Al-MCF) was successfully achieved using a simple, fast and efficient reactive milling (mechanochemical) method. Upon preparation, catalysts were characterized by $N_2$-physisorption, elemental analysis, Transmission Electron Microscopy (TEM) and X-ray diffraction (XRD). The catalytic activity of different Pd/Al-SBA-15 and Pd/Al-MCF materials was investigated in the hydrogenation of *p*-Nitrophenol (PNP) to *p*-Aminophenol (PAP) using $NaBH_4$ as reducing agent. Significant differences in catalytic activity for the prepared catalysts were observed, with a superior catalytic activity of Pd/Al-MCF as compared to Pd/Al-SBA-15. Furthermore, investigations on external mass-transfer limitations of the reaction conducted with two selected supported Pd catalysts were conducted and discussed.

## Introduction

Metallic nanoparticles have become a research topic of relevance in modern nanoscience due to their unique physico-chemical properties as well their important implications in catalytic processes.[1-5] As an example, the first work by Haruta *et al.*[6] on Au nanoparticles for CO oxidation was followed by a number of reports detailing the design of supported nanoparticle systems for heterogeneously catalyzed applications. In this regard, metal nanoparticles can be incorporated and supported in a number of porous supports using diverse techniques ranging from conventional methodologies such as incipient wetness impregnation or co-precipitation to more innovative protocols including ball milling,[7] microwave-assisted irradiation[8] or supercritical fluid reactive deposition (SFRD).[9, 10]

Functionalized nanoporous materials represent an important class of nanomaterials and a research area in which fascinating developments have been achieved in past decades.[11] One of current major challenges in the synthesis of nanoporous materials deals with the design and controllable preparation of a suitable porous structure with several complementary functions for improved activity, selectivity and stability in catalytic applications.[12-15] Ordered mesoporous SBA-15 silicas and mesostructured cellular foams (MCFs) are examples of porous solids able to provide most of the aforementioned requirements for an advanced catalytic material.

Mesostructured cellular foams (MCFs) comprise a novel type of porous silica-type materials comprising a three-dimensional structure with hydrothermally robust ultra-large mesopores (up to 50 nm).[16-18] In terms of textural and framework properties, MCFs are composed of uniform spherical cells interconnected by window pores with a narrow size distribution.[16] Owing to their 3D mesopore system with pore sizes substantially larger than those of SBA-15, these materials can be, in principle,

considered to be highly promising candidates as catalytic supports, potentially providing a faster diffusion of the reactants and products in chemical processes as well as a stable porous phase.[17,19] However, further functionalization is generally required to incorporate catalytically active sites into these materials due to their inherent inertness.[20-24]

The direct incorporation of metals into the structure of nanoporous silica supports can be achieved via isomorphic substitution of Si with Al, enabling the generation of acid sites. Interestingly, there is limited information about the functionalization of MCF materials for catalytic applications, with very few reports dealing with direct synthetic protocols, e.g., via isomorphic substitution.[25]

In this work, we present a simple, rapid and efficient alternative for metal incorporation into nanoporous supports based on reactive milling (mechanochemistry). Advanced bifunctional nano-molecular entities can be efficiently designed using this methodology, which provides accessibility to the active site of the catalysts in the reactions that require bifunctional catalysts i.e., acid sites as well as metal sites. This would be advantageous, e.g., for the conversion of biomass to liquid fuels and chemicals. The proposed methodology has been illustrated for the particular preparation and stabilization of Pd nanoparticles within two nanoporous aluminosilicate materials, i.e., Al-SBA-15 and Al-MCF. In addition to catalysts preparation, the catalytic activity of the prepared catalysts was assessed in greener aqueous-phase hydrogenations of aromatic compounds, using the low temperature (278 K) reduction of $p$-Nitrophenol (PNP) to $p$-Aminophenol (PAP) in presence of $NaBH_4$ as model test reaction.[26]

**Experimental Section**

*Catalyst preparation*

The synthesis of parent Al-SBA-15 support has been performed using a previously reported procedure[27] as follows: 25.2 g of structure directing agent (Pluronic P123, Sigma Aldrich) were dissolved in 472.5 mL of 2M HCl and 236 mL of distilled water. 54.9 g of (tetraethyl orthosilicate (TEOS), ABCR) and 2.8 g of aluminum isopropoxide (≥98% purity from Aldrich, corresponding to an Si/Al ratio 20 in the gel) were then added to the mixture and stirred at room temperature for 24 h at pH ≈ 2. This mixture was aged at 373 K for 24 h. The precipitated solid was filtered off, washed and dried at 373 K for 12 h prior to calcination at 873 K.

The synthesis of parent Al-MCF has comparably been adapted from Lettow *et al.* [17] 4.0 g Pluronic P123 (BASF, molecular weight = 5800) was dissolved in 22.8 g HCl (37%) and 75 mL distilled water. In contrast to the original procedure, 16 g 1,3,5 trimethylbenzene (MERK) (corresponding to a TMB/P123 ratio = 4) and 2.8 g aluminum isopropoxide were added to the solution. As silicon source, 8.8 g TEOS (ABCR) was added dropwise to the solution. Upon stirring at 310 K for 24 h and aging at 393 K in a closed Teflon bottle, the final obtained solid was filtered off, washed and calcined at 813 K to remove the remaining organics.

Supported Pd on Al-SBA-15 and Al-MCF catalysts were subsequently prepared using an efficient mechanochemical deposition of Pd onto the support material. In this method, certain amounts of the support (Al-SBA-15 and Al-MCF) and a metal precursor (palladium (II) acetate, Sigma Aldrich) in the solid phase were milled together for 5 min at 350 rpm using a planetary ball mill (Retsch PM 100 model). For comparison, a supported Pd on Al-MCF catalyst was prepared via conventional

incipient wetness impregnation (IWI) with 0.5 wt.% of Pd as an aimed loading. The required amount of tetraamminepalladium (II) nitrate (Sigma Aldrich) was dissolved in distilled water and added dropwise with continuous stirring to the support, i.e., Al-MCF. The obtained catalysts were calcined for 4 h at 723 K and reduced under a flow of $H_2$ (2 mL min$^{-1}$) in $N_2$ (8 mL min$^{-1}$). The incorporation procedure is illustrated in Figure 1.
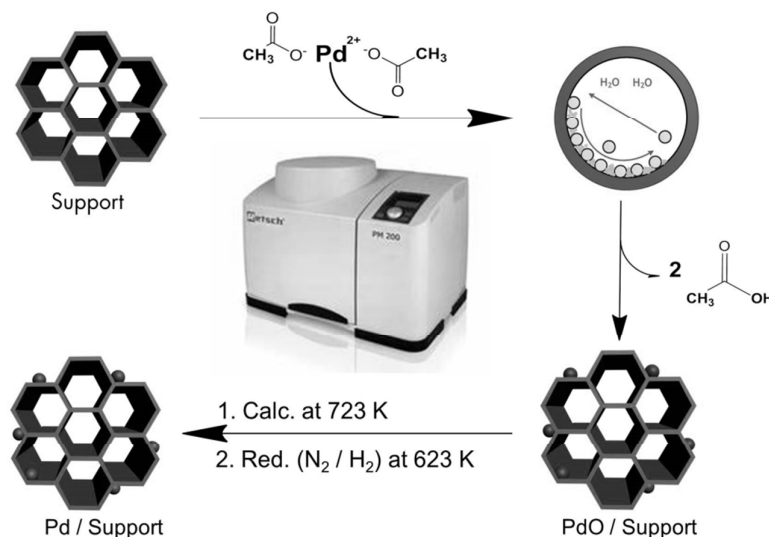


Figure 1. Scheme representing the incorporation of Pd nanoparticles onto ordered nanoporous material (Al-SBA-15 and Al-MCF) via ball milling.

*Characterization techniques*

The prepared catalysts were characterized by $N_2$-physisorption, elemental analysis, transmission electron microscopy (TEM) and X-ray diffraction (XRD). The specific surface area, pore volume and pore size distribution were determined using a micrometrics ASAP 2010 apparatus. The metal content was determined by optical emission spectroscopy with inductively coupled plasma (ICP-OES) after dissolution of the sample in aqueous $HNO_3$/HF solution using a Vario EL-Heraeus microanalyzer. Transmission Electron Micrographs (TEM) of the support materials and the catalysts

were recorded on a JEOL JEM 2010HR instrument operated at 300 kV. Samples were

suspended in ethanol and deposited straightaway on a copper grid prior to analysis.

EDX for elemental analysis could also be recorded on the same apparatus. Additionally,

XRD patterns were recorded within $2\theta = 4 - 90°$ range using a Siemens, D5000

diffractometer ($0.05°$ counts per step) and Cu-K$\alpha$ radiation ($\lambda = 0.154$ nm).

*Catalytic test reaction*

The catalytic hydrogenation of PNP to PAP was carried out in a 100 mL batch reactor at

279 K (ambient pressure, 1300 rpm stirring speed). Figure 2 depicts the catalytic

experimental setup. Details of the experimental procedure may be found elsewhere.[26] In

brief, 5 mL of an aqueous solution of NaBH$_4$ ($0.60$ mmol$^{-1}$) were added to 45 mL of an

aqueous solution of PNP ($0.18$ mmol$^{-1}$). The reaction was started by introducing 0.07 g

of the reduced catalyst. PNP concentration changes were monitored via on-line UV-vis

spectroscopy (AvaSpec-3648, optical path length: 5 mm) at a wavelength of 400 nm.

The initial reaction rate ($r_0$) was calculated by assuming first order reaction from the

linear decrease of PNP concentration after the addition of the catalyst.



Figure 2. Experimental setup for hydrogenation of PNP with NaBH$_4$ to PAP with online
UV-vis spectrometer.

**Results and Discussion**

*Material preparation and characterization*

Pd nanoparticles have been incorporated into the support via ball milling, following a previously established methodology[7], in two steps, namely hydrolysis of the metal precursor to generate $Pd^{2+}$ species (PdO, upon calcination) followed by subsequent reduction to $Pd^0$ nanoparticles. The protocol allows the incorporation of an uniform distribution of Pd nanoparticles mostly on the surface of the support, with a contribution within the pores of the materials as previously reported.[27, 28]

Textural properties of the synthesized materials are summarized in Table 1 and Figure 3. In all cases, isotherms were found to be of type IV with hysteresis loops of H1 type according to the IUPAC classification. These correspond to mesoporous materials with pores of the same cross section (for instance, cylindrical or hexagonal). Pore-filling steps in adsorption and desorption curves were sharp, corresponding to a narrow pore size distribution. Specific surface area ($S_{BET}$), specific surface area for micropores ($S_{mi}$), specific pore volume for micropores and mesopores ($V_{mi}$ and $V_{me}$), total pore volume ($V_{tot}$) at relative pressure 0.99, and pore diameter ($d_p$) and window diameter ($d_w$) obtained from desorption branch of the isotherms are summarized in Table 1.

No major changes could be observed in terms of textural properties upon Pd incorporation into Al-SBA-15 or Al-MCF. Specific surface areas generally decreased with the amount of incorporated Pd (up to a maximum of 20 %) as expected, with an interesting decrease in the micropore contribution for Al-SBA-15 materials (Table 1, $S_{mi}$ column). The decrease in micropore surface area may be due to micropore filling with Pd, although a contribution of micropore destruction from the milling process cannot be ruled out. Comparably, an unexpected increase in micropore surface area

could be observed for ball-milled Al-MCF materials which can be attributed to micropore opening after milling of unnacessible micropores already present in the original Al-MCF (unquantified via adsorption in the parent material). Pore diameters were only slightly reduced upon Pd incorporation, i.e. minimum generation of Pd nanoparticles within the pores of the materials, without any significant changes in $V_{tot}$. These findings again confirmed the predominant deposition of Pd NPs on the external surface of the support in good agreement with previous results of Luque *et al*.[7, 11, 28]

**Table 1.** Textural properties of materials synthesized in this work include specific surface area ($S_{BET}$), specific surface area for micropores ($S_{mi}$), pore volume for micropores and mesopores ($V_{mi}$ and $V_{me}$), total pore volume ($V_{tot.}$), window diameter ($d_w$) and Pd content and Al content (measured by ICP-OES).

| Materials | $S_{BET}$ $(m^2g^{-1})$ | $S_{mi}$ $(m^2g^{-1})$ | $V_{mi}$ $(cm^3g^{-1})$ | $V_{me}$ $(cm^3g^{-1})$ | $V_{tot.}$ $(cm^3g^{-1})$ | $d_p$ (nm) | $d_w$ (nm) | Al content (wt.%) |
|---|---|---|---|---|---|---|---|---|
| Al-SBA-15 | 728 | 230 | 0.09 | 0.5 | 0.6 | 9.8 | - | 2.0 |
| 0.2 Pd/Al-SBA-15 | 715 | 113 | 0.04 | 0.5 | 0.6 | 7.3 | - | 1.7 |
| 2.0 Pd/Al-SBA-15 | 736 | 105 | 0.04 | 0.6 | 0.7 | 6.8 | - | 2.2 |
| Al-MCF | 693 | 148 | 0.06 | 2.1 | 2.1 | 28.0 | 15.0 | 0.2 |
| 0.4 Pd/Al-MCF | 616 | 152 | 0.06 | 2.0 | 2.1 | 26.0 | 14.0 | 0.8 |
| 2.1 Pd/Al-MCF | 579 | 175 | 0.07 | 2.0 | 2.1 | 25.0 | 14.0 | 0.2 |

The amount of Pd loading on the support was determined by elemental analysis via ICP-OES. Catalysts studied in this work were originally prepared with 0.5 wt.% and 2.0 wt.% aimed Pd loadings, which correlated fairly well with actual Pd loadings in the final materials. Only for the case of 0.5 Pd/Al-SBA-15, the final Pd loading was found to be rather low (0.2 wt.%). Pd and Al content in all materials are included in Table 1.
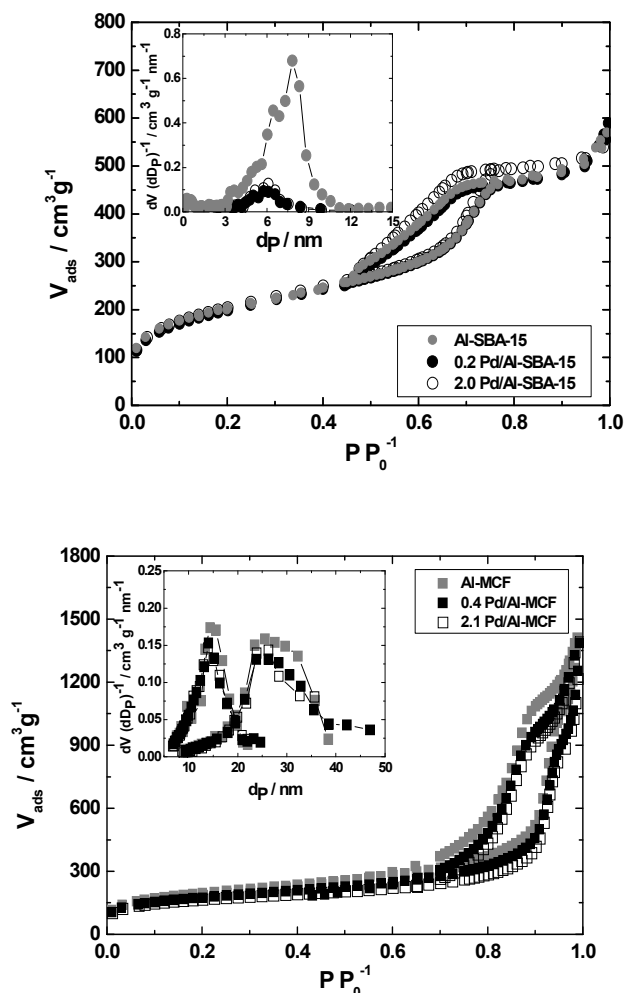
**Figure 3**. Nitrogen physisorption isotherms at 77 K and pore width distribution determined using the BJH method on the desorption branch of the isotherm for Al-SBA-15, 0.2 Pd/Al-SBA-15 and 2.1 Pd/Al-SBA-15 (top plot); Al-MCF, 0.4 Pd/Al-MCF and 2.1 Pd/Al-MCF (bottom plot).

TEM images for 0.2 Pd/Al-SBA-15 and 0.4 Pd/Al-MCF have been shown in Figure 4. Pd-containing Al-SBA-15 materials exhibited the characteristic highly ordered hexagonal arrays of mesopores with large uniform pore diameters and a well preserved structure after ball milling and Pd incorporation. In contrast, TEM images revealed a

disordered array of silica sturts containing uniform spherical cells interconnected by windows with a narrow size distribution, all characteristic of MCF materials.[29] Images did not allow a clear visualization of Pd nanoparticles (Figure 4) which in any case rules out the presence of large Pd clusters in the materials. XRD patterns (Figure S1 in ESI) of the prepared catalysts did not reveal any characteristic Pd diffraction lines (even for samples with 2.0 wt.% Pd loading), as expected due to the low Pd content in the materials and their high dispersion on the supports. These results were in good agreement with TEM results which did not show any clear Pd nanoparticles in the materials.
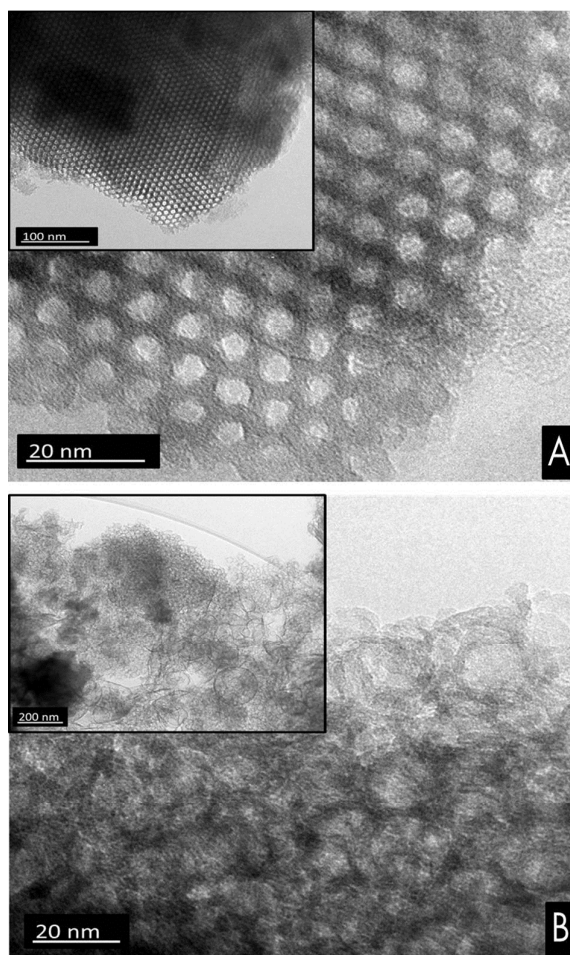


**Figure 4.** Representative TEM images of prepared catalysts (A) 0.2 Pd/Al-SBA-15 (B) 0.4 Pd/Al-MCF.

*Catalytic activity*

Catalytic experiments of Pd-containing Al-SBA-15 and Al-MCF materials in the aqueous hydrogenation of PNP to PAP at 278 K using $NaBH_4$ as reducing agent were conducted. Results are depicted in Figures 5 to 8. PNP adsorption on Al-SBA-15 and Al-MCF supports materials as well the effects of the support on PNP hydrogenation were initially investigated. The addition of the support material did not have any significant influence on the observed PNP concentration, ruling out any significant adsorption effects on the catalytic measurements. Moreover, experiments in the presence of parent Al-SBA-15 and Al-MCF supports and in the absence of any solid material (blank runs) gave no catalytic activity, i.e., no PNP concentration change in solution was observed. Upon addition of the Pd-containing catalysts, PNP concentration decreased linearly with time, reaching a maximum conversion after less than 5 min. Figure 5 summarizes the results of concentration vs. time behavior for the investigated catalysts. Almost quantitative conversion could be achieved for 2.0 Pd/Al-SBA-15 and 2.1 Pd/Al-MCF in a very short period of time (typically less than 2 minutes).
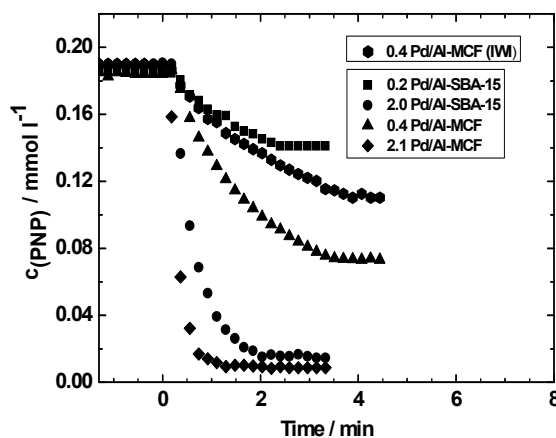


**Figure 5.** Concentration of PNP as a function of time for different supported Pd catalysts in the hydrogenation of PNP to PAP using $NaBH_4$ as reducing agent. ($c_{(PNP)}$ =

0.18 mmol L$^{-1}$, c$_{(NaBH4)}$ = 0.60 mmol L$^{-1}$, T = 279 K, stirring speed = 1300 min$^{-1}$, m$_{catalyst}$ = 0.07 g).

As expected, rates of reactions were slower for lower Pd loaded materials, although a highly promising ca. 60% conversion was achieved for 0.4 Pd/Al-MCF after 5 minutes of reaction (Figure 5).

Note that on catalysts with lower loading and from IWI, a complete conversion of PNP to PAP was not achieved. This is, however, not due to catalyst deactivation, but due to incomplete utilization of the hydrogen from NaBH4 decomposition in the PNP hydrogenation. In fact, complete conversion can be reached also on these less active catalysts, if more NaBH4 is added to the reaction mixture (see Figure S3 in ESI).[26]

Initial reaction rates were subsequently calculated by assuming a first order reaction, from the linear decrease of PNP concentration as function of time after addition of the catalyst (Figure 6). The generally higher reaction rate for 2.0 Pd/Al-SBA-15 (0.220 mmol l$^{-1}$ min$^{-1}$) as compared to 0.2 Pd/Al-SBA-15 (0.019 mmol l$^{-1}$ min$^{-1}$) and 2.1 Pd/Al-MCF (0.306 mmol l$^{-1}$ min$^{-1}$) as compared to 0.4 Pd/Al-MCF (0.137 mmol l$^{-1}$ min$^{-1}$) can be easily correlated to their respectively larger Pd content. A linear correlation of such higher rates of reaction with the quantity of Pd in the materials was not observed which may be due to more severe mass-transfer limitations for increasing initial reaction rates (see below). The initial reaction rates determined in this work were comparably superior to those previously reported by Goepel *et al.* using similarly loaded supported Pt catalysts.[26] Results were also consistent and in good agreement with findings from El-Sheikh *et al.*[29], who also reported a higher catalytic performance of supported Pd as compared to supported Pt catalysts in NaBH$_4$-mediated PNP

hydrogenation. However, Goepel *et al.*[26] observed a limitation of reaction kinetics by internal mass-transfer effects. The increase in initial reaction rate compared to the supported Pt-catalysts used in their study (prepared by electrostatic adsorption) can also be understood as overcoming internal mass-transfer limitations via preferential deposition of Pd on the external surface of the catalyst,[28] illustrating the advantages of mechanochemical catalyst preparation.
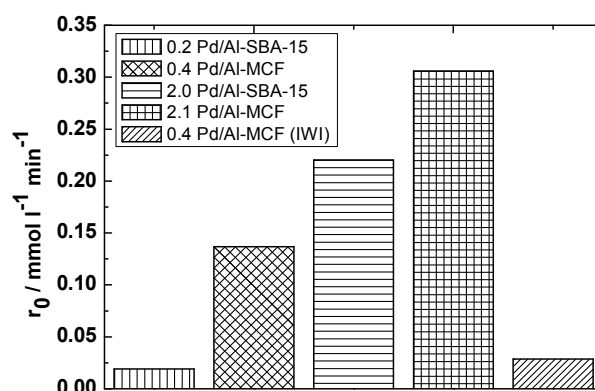


**Figure 6.** Initial reaction rates in the hydrogenation of PNP to PAP using $NaBH_4$ as reducing agent for different supported Pd catalysts. ($c_{(PNP)}$ = 0.18 mmol l$^{-1}$, $c_{(NaBH4)}$ = 0.60 mmol l$^{-1}$, T = 279 K, stirring speed = 1300 min$^{-1}$, $m_{catalyst}$ = 0.07 g).

In order to compare catalytic results achieved with ball milling-prepared supported Pd nanoparticles with conventionally prepared catalysts, a similarly low loaded 0.4 Pd/Al-MCF catalyst prepared via IWI was used. As expected, the conversion was much faster when using 0.4 Pd/Al-MCF (Figure 5, dotted line) prepared by ball milling compared to the catalyst with the same Pd loading obtained by IWI. Only the conversion over the catalyst 0.2 Pd/Al-SBA-15 prepared via ball milling is slower. This can be attributed to its lower noble metal loading. These findings are in good agreement

with previous results from the group[27, 28] and confirm the remarkable possibilities of mechanochemically synthesized materials as advanced catalysts.

Mass-transfer limitations in the aqueous phase were finally evaluated in the systems. With this purpose, the stirring speed was varied for the conversion using two selected catalysts, i.e., 0.2 Pd/Al-SBA-15 and 0.4 Pd/Al-MCF. A linear correlation between stirring speed and initial rate of reaction was observed for both catalysts (Figure 7), confirming that the hydrogenation of PNP using $NaBH_4$ as a reducing agent is limited by external mass-transfer. Similarly, external mass-transfer limitations were also found for very active Pt catalysts supported on mesoporous silica gel.[26] These results may indicate that the Pd particles are highly dispersed (< 2 nm) on the external surface of the support. The fact that the initial reaction rate is higher for the higher metal loadings is also consistent with the above mentioned conclusion that most of Pd particles are located at the external surface in the supports. For both lower and higher Pd loading, Al-MCF-based catalysts were more active as compared to Al-SBA-15.

In view of the observed external mass-transfer limitations, Al-MCF-base catalysts can be proposed to either contain smaller Pd particles, i.e., supports a higher Pd dispersion, or it comprises smaller or differently shaped grains resulting in a thinner diffusion layer and consequently a less pronounced external mass-transfer limitation of the reaction rates.

The stability of synthesized Pd catalysts was also investigated in this work. ICP/OES of both filtrate (no Pd leaching detected in solution, <0.5 ppm) as well as the reused catalyst (0.4 wt.% Pd in the reused catalyst, identical to 0.4 wt.% Pd measured in fresh Pd/Al-MCF) supports the high stability of recyclability of mechanochemically synthesized nanocatalysts in aqueous room temperature catalytic processes, in good agreement with recent reports.[29]
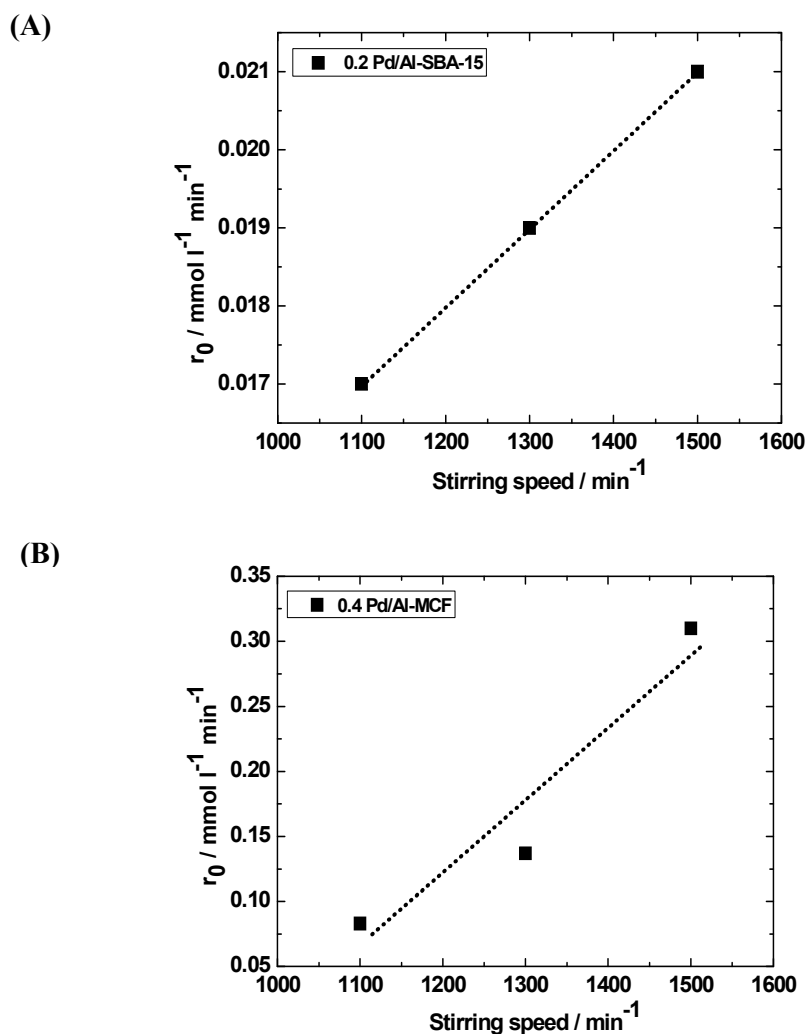
**(A)**



**(B)**



**Figure 7.** Initial reaction rate ($r_0$) dependence with stirring speed in the hydrogenation of PNP to PAP using $NaBH_4$ as a reducing agent (A) 0.2 Pd/Al-SBA-15 and (B) for 0.4 Pd/Al-MCF. ($c_{(PNP)}$ = 0.18 mmol $l^{-1}$, $c_{(NaBH4)}$ = 0.60 mmol $l^{-1}$, T = 279 K, stirring speed = 1300 $min^{-1}$, $m_{catalyst}$ = 0.07 g).

**Conclusions**

Advanced bifunctional nanomaterials Pd/Al-SBA-15 and Pd/Al-MCF have been successfully designed using a facile and straightforward route based on a dry milling mechanochemical protocol as innovative preparation strategy. The catalytic activity as

well as the mass-transfer limitations of the prepared catalysts have been successfully investigated in the hydrogenation PNP to PAP as a model reaction. Significant differences in catalytic activity for the prepared catalysts were observed, with an optimum activity achieved for 2.1 Pd/Al-MCF and negligible activities obtained for similar materials prepared via conventional incipient wetness impregnation (IWI) method. The new generation of advanced mechanochemically synthesized materials is envisaged to pave the way to the utilization of simple, stable and highly active nanomaterials for challenging catalytic processes (e.g. aqueous chemistries) within future biorefineries and biomass processing.
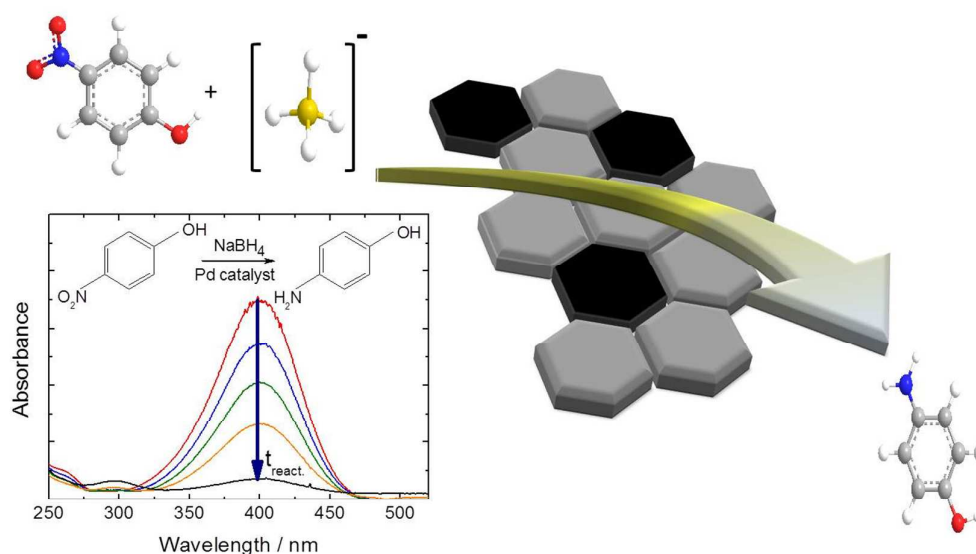
**References**

[1]    P. Hervés, M. P. Lorenzo, L. M. L. Marzán, J. Dzubiella, Y. Lu, M. Ballauff, *Chem. Soc. Rev.* **2012,** *41*, 5577- 5587.

[2]    A. A. Ismaila, A. Hakki, D. W. Bahnemann, *J. Mol. Catal. A: Chem.* **2012**, *358*, 145-151.

[3]    Y. Mei, Y. Lu, F. Polzer, M. Ballauff, *Chem. Mater.* **2007,**  *19*, 1062-1069.

[4]    Y. Lu, Y. Mei, M. Drechsler, M. Ballauff, *Angew. Chem. Int. Ed.* **2006**, *45* 813-816.

[5]    W. Schäartl, *Nanoscale* **2010**, *2*, 829-843.

[6]    M. Haruta, T. Kobayashi, H. Sano, N. Yamada, *Chem. Lett.* **1987**, *2*, 405-408.

[7]    A. Pineda, A. M. Balu, J. M. Campelo, A. A. Romero, D. Carmona, F.   Balas, J. Santamaria, R. Luque*, ChemSusChem* **2011***, 4,* 1561-1565*.*

[8]    A. M. Balu, D. Dallinger, D. Obermayer, J. M. Campelo, A. A. Romero, D. Carmona, F. Balas, K. Yoshida, P. L. Gai, C. Vargas, C. O. Kappe, R. Luque, *Green Chemistry* **2012**, *14*, 393-402.

[9]    J. Morère, M. J. Tenorio, M. J. Torralvo, C. Pando, J. A. R. Renuncio, A. Cabañas, *J. Supercrit. fluids* **2011**, 65, 213-222.

[10]   M. Lindo, A. J. Vizcaíno, J. A. Calles, A. Carrero, *Int. J. Hydrogen Energy* **2010**, *35*, 5895-5901.

[11]   M. Ojeda, A.M. Balu, V. Barrón, A. Pineda, A. Garcia, A. A. Romero, R. Luque, *J. Mater. Chem. A* **2014,** *2*, 387-393.

[12]   V. Salgueiriño-Maceira, M. A. Correa-Duarte, *Adv. Mater.* **2007,** *19*, 4131-4144.

[13]   P. Majewski, B. Thierry, *Crit. Rev. Solid State Mater. Sci.* **2007**, *32,* 203-215.

[14]    P. Tallury, K. Payton, S. Santra, *Nanomedicine* **2008**, *3*, 579-592.

[15]   J. Kim, Y. Piao, T. Hyeon, *Chem. Soc. Rev.* **2009**, *38*, 372-390.

[16]   P. S. Winkel, W. W. Lukens, D. Zhao, P. Yang, B. F. Chmelka, G. D. Stucky, *J. Am. Chem. Soc.* **1999**, *121*, 254-255

[17]   J. S. Lettow, Y. J. Han, P. S. Winkel, P. Yang, D. Zhao, G. D. Stucky, J. Y. Ying, *Langmuir* **2000**, *16*, 8291-8295

[18]   Q. Li, Z. Wu, D. F. Eng, B. Tu, D. J. Zhao, *J. Phys. Chem. C* **2010**, *11*, 5012-5019.

[19]   Y. J. Han, J. T. Watson, G. D. Stucky and A. Butler, *J. Mol. Catal. B* **2002**, *1*, 1-8.

[20]   C. Li, Y. Wang, Y. Guo, X. Liu, Y. Guo, Z. Zhang, Y. Wang, G. Lu, *Chem. Mater.* **2007**, *19,* 173-178.

[21]   Z. Lihui, H. Jun, X. Songhai, L Honglai, *Chin. J. Chem. Eng.* **2007**, *15*, 507-511.

[22]   A. Galarneau, H. Cambon, F. Di Renzo, F. Fajula, *Langmuir* **2001**, *17,* 8328-8335.

[23]   Y. M. Liu, J. Xu, L. C. Wang, Y. Cao, H. Y. He, K. N. Fan, *Catal Lett.* **2008**, 125, 62-68.

[24]   R. Fazaeli, H. Aliyan, M. A. Ahmadi, S. Hashemian, *Catal. Commun.* **2012**, *29,* 48-52.

[25]   L. Hermida, A. Abdullah, A. Mohamed, *Mater. Sci. Appl.* **2013**, 4, 52-62.

[26]   M. Goepel, M. Al-Naji, P. With, G. Wagner, O. Oeckler, D. Enke, R. Gläser, *Chem. Eng. Technol.* **2014**, *37*, 551-554.

[27]   a) A. M. Balu, A. Pineda, K. Yoshida, J. M. Campelo, P. L. Gai, R. Luque, A. A. Romero, *Chem. Commun.* **2010**, *46*, 7825-7827; b) A. M. Balu, A. Pineda, D. Obermayer, A. A. Romero, C. O. Kappe, R. Luque, *RSC Adv.* **2013**, *3*, 16292-16295.

[28]  a) M. Ojeda, A. M. Balu, V. Barron, A. Pineda, A. Garcia, A. A. Romero, R. Luque, *J. Mater Chem. A* **2014**, *2*, 387-393; b) M. Ojeda, A. Pineda, A. A. Romero, V. Barron, R. Luque, *ChemSusChem* **2014**, 10.1002/cssc.201400055.

[29]  S. M. El-Sheikh, A. A. Ismail, J. F. Al-Sharab, *New J. Chem.* **2013**, *37*, 2399-2407.

The preparation of supported Pd nanoparticles on porous materials was successfully achieved using a simple fast and efficient reactive milling (mechanochemical) method. The catalytic activity of different Pd/Al-SBA-15 and Pd/Al-MCF materials was investigated in the hydrogenation of *p*-Nitrophenol (PNP) to *p*-Aminophenol (PAP) using NaBH$_4$ as a reducing agent.